The Journal of Adhesion, 81:723–750, 2005

ISSN: 0021-8464 print/1545-5823 online
DOI: 10.1080/00218460500187715

Taylor & Francis
Taylor & Francis Group

Probing the Physics of Slip–Stick Friction using a Bowed String

R. T. Schumacher
Physics Department, Carnegie Mellon University, Pittsburgh, Pennsylvania, USA

S. Garoff
Physics Department and Center for Complex Fluids Engineering, Carnegie Mellon University, Pittsburgh, Pennsylvania, USA

J. Woodhouse
Cambridge University Engineering Department, Cambridge, UK

Slip–stick vibration driven by friction is important in many applications, and to model it well enough to make reliable predictions requires detailed information about the underlying physical mechanisms of friction. To characterize the frictional behavior of an interface in the stick–slip regime requires measurements that themselves operate in the stick–slip regime. A novel methodology for measurements of this kind is presented, based on the excitation of a stretched string "bowed" with a rod that is coated with the friction material to be investigated. Measurements of the motion of the string allow the friction force and the velocity waveform at the contact point to be determined by inverse calculation. These friction results can be correlated with microscopic analysis of the wear track left in the coated surface. Results are presented using rosin as a friction material. These show that "sticking" involves some temperature-dependent shear flow in the friction material, and that the exact definition of the states of "sticking" and "slipping" is by no means clear-cut. Friction force during slipping shows complex behavior, not well correlated with variations in sliding speed, so that other state variables such as temperature near the interface must play a crucial role. A new constitutive model for rosin friction, based on the repeated formation and healing of unstable shear bands, is suggested.

Keywords: Adhesion; Creeping friction; Friction-driven autonomous oscillations; Interfacial friction; Kinetic friction; Stick–slip oscillation

Received 14 October 2004; in final form 15 March 2005.

One of a collection of papers honoring Manoj K. Chaudhury, the February 2005 recipient of The Adhesion Society Award for Excellence in Adhesion Science, sponsored by 3M.

Address correspondence to Robert T. Schumacher, Department of Physics, Carnegie Mellon University, Pittsburgh, PA 15213, USA. E-mail: rts@andrew.cmu.edu

INTRODUCTION

The measurement of friction force at an interface can be important for many reasons, from understanding the fundamental physics of friction to characterizing the friction and wear properties of particular interfaces relevant to machines and other applications. For many of these applications, ranging from vehicle brakes through microelectromechanical systems (MEMS) to the strings of a violin, one reason for interest in friction is that vibration may be caused by frictional interaction (see, for example, references 1 and 2). This vibration may be wanted or unwanted, but in either case there is a need to understand, predict, and control it. Engineering-based problems of this kind may seem rather old-fashioned by comparison with the novel applications to, for example, rock mechanics or biological systems, which have been the focus of much attention in recent friction research (see, for example, references 3 and 4). However, many unsolved problems remain in this area that are significant both for fundamental physical understanding and for technological applications.

Characterizing the constitutive law that determines the friction force currently presents the greatest challenge in modeling friction-driven vibration. In many technological disciplines it is still common to assume extremely naive models of friction, which when subjected to experimental scrutiny turn out not to give predictions that are sufficiently reliable for design purposes. In recent years various more-sophisticated friction models have been proposed (such as the "rate and state" models, see, for example, references 4 and 5) that give a better qualitative match to observed frictional behavior in certain settings. However, when detailed tests have been made it has generally been found that none of these models is yet capable of quantitative prediction of the stability threshold and transient details of frictionally excited vibration, especially when it occurs at high frequency [2, 6–9]. For example, to the best of the authors' knowledge it is not possible to use any current finite-element package to obtain reliable predictions of when a vehicle braking system will squeal.

There are many ways to measure friction. Most types of apparatus are designed to impose a state of steady sliding and then determine the resulting shear force across the interface. (The words "slipping" and "sliding" are used interchangeably.) Factors such as pressure, temperature, and humidity may be varied to give a fuller characterization of the tribological behavior. However, if one's aim in characterizing friction is to predict and control friction-excited vibration, then such a strategy is inadequate. The friction force during self-excited vibration, often at kilohertz frequencies, will in general behave

differently from anything one might deduce from steady-sliding measurements (see, for example, references 6 and 9). To obtain sufficient data to motivate, validate, and calibrate accurate constitutive laws it is necessary to augment steady-sliding tests with controlled measurements using an apparatus that itself operates in the stick–slip regime, or which imposes some other high-frequency dynamic variation. Such measurements pose new challenges to the experimenter. No single apparatus can be expected to provide all the necessary information, and this article describes one promising recent approach that complements other methods.

A bowed violin string is a familiar example of vibration excited by friction. In a musical context, the friction behavior is given and the musician is interested in what kind of string motions, and hence sounds, can be produced. In this work, we turn the idea around. Using an apparatus based on a well-characterized stretched string excited by a "bow" coated with a layer of the friction material to be studied, observations of the string motion are used to infer the friction force, which is hard to measure directly under these interfacial conditions. The evidence from the measurement of friction force can be supplemented by microscopic examination of the damage track created by a single pass of the bow over the vibrating string. Details of these tracks can be correlated with the waveforms of measured force and velocity, and standard identification techniques (see, for example, reference 10) can then assist in identifying the physical events that give rise to the dynamic friction force.

The results, taken together with other dynamic tests on the same friction material [6, 7, 9], reveal that none of the current theoretical models of friction capture the full range of observed phenomena. These results give useful clues about how models need to be enhanced before one could hope to have a robust, predictive model for the occurrence of friction-driven vibration. This article is focused on experimental methods and results, but complementary studies using simulation with various candidate frictional constitutive laws are being carried out, and some results have already been published [6, 7, 9].

EXPERIMENTAL APPARATUS AND METHODS

Background of Inverse Measurement Methods

The first measurements of friction force by an "inverse" method based on stick–slip vibration were reported by Bell and Burdekin [11] and Brockley and Ko [12]. They both used systems that were essentially single-degree-of-freedom oscillators. For such a system, once the mass,

stiffness, and damping have been determined by a calibration measurement, the equation of motion of the oscillator can be used directly to convert measured motion of the mass into a time-varying friction force.

These early measurements revealed a phenomenon that has subsequently been confirmed in many other systems. Measurements based on steady sliding often show a coefficient of friction that varies with sliding speed. It is a natural step to suppose that this relation carries over directly to the context of dynamic friction, so that the coefficient of friction is determined entirely by instantaneous sliding speed. If the coefficient of friction falls with increasing sliding speed, unstable self-excited vibration can occur, and this has been regarded for many years as a major mechanism for such vibration (see, for example, the review [1]). However, when dynamic friction measurements were made and the friction force $F(t)$ was plotted against the velocity $v(t)$, a hysteresis loop was seen. This shows immediately that sliding speed is not the only state variable influencing the friction force.

An example is shown in Figure 1, taken from work by Smith and Woodhouse [6] using a single-degree-of-freedom test rig similar in principle to the earlier work. The interfacial frictional material here is rosin, a natural resinous material whose main active ingredient is abietic acid [13]. This is the material used on violin bows and in many other contexts where an antilubricant or tackifier is needed, making it an interesting frictional material to investigate because it has quite extreme properties. The solid curve shows the experimentally determined trajectory traced out in the F-v plane. The dashed curve shows the result of steady-sliding measurements on the same frictional material under similar contact conditions. The dashed curve shows a vertical portion, because during sticking the force between the two surfaces can take any value up to the limit of static friction. Once sliding has begun, the coefficient of friction falls dramatically. The dynamical measurement shows results that are very different. An almost-vertical "sticking" portion can be seen, slightly obscured by loops that are (at least in large part) a measurement artifact [6]. During sliding, a loop is traced out in a counterclockwise direction. No part of this loop lies close to the dashed curve nor does its tangent slope correspond. Loops of this kind seem to be ubiquitous: similar results are shown later using the bowed-string measurement apparatus.

Smith and Woodhouse [6] proposed a thermal-based constitutive model to account for results such as those shown in Figure 1, in which friction force is determined not by sliding speed but by temperature in the interfacial region. This model is related to the "rate and state" models of friction, but, whereas those models are often empirically

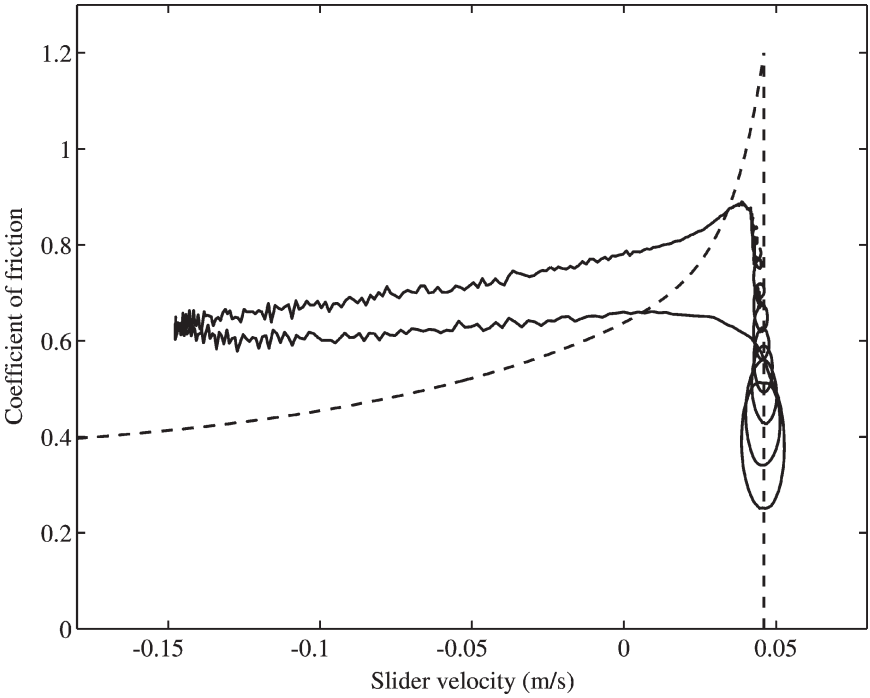

FIGURE 1 Friction force *versus* slider velocity. Solid line: results measured in a dynamic experiment [6] showing a hysteresis loop that is traversed in the counterclockwise direction; dashed line: measured result from a steady-sliding test under identical contact conditions. The bow speed was 0.042 m/s, as indicated by the vertical dashed line. The "sticking" portion of the dynamically measured curve shows loops because the measuring sensor was not exactly at the bow-string contact point.

formulated, in this case the "state" has a simple physical interpretation as instantaneous temperature in the contact. The heat generated by friction induces changes in the mechanical properties of the material at the frictional contact. Simulations using an accurate dynamical model plus appropriate material properties produced a variation of frictional force that was broadly similar to that found in their experiments [6, 7]. However, "broadly similar" is not good enough as a basis to claim that the problem has been solved, and the detailed results make it clear that the true frictional model needs to be more complicated [7, 9]. An enhanced model requires a range of controlled experimental data to underpin it.

Bowed-String Apparatus

We report here on experiments similar to references 6, 11, and 12, but employing a system that shows a wider range of dynamical behavior and that, thus, allows significantly different regions of parameter space to be probed. Motivated by the considerable knowledge of the dynamics of bowed strings (*e.g.*, references 14 and 15), we use a string under tension that is excited using a glass rod coated with the chosen friction material, rosin for the results reported here. The basic apparatus and method have been described previously [16]. A brief review is given to render this article self-contained, and then new extensions and results are described: the major additions are a way to measure the average friction force, the use of additional regimes of oscillation, new results deriving from an exploration of the effect of ambient temperature, and the calculation of the energy flows during stick–slip vibration.

The glass rod is coated with commercial rosin of a type used for bass violins. A homogeneous layer, with thickness on the order of microns, was applied by dissolving the rosin in xylene, and then immersing and withdrawing the rod at a constant velocity from the solution. The rod was allowed to dry for several days before being used. We have also explored a dry application method, in which the rosin is applied in a powder form. The initial application resulted in a rather rough surface, with a friction force about twice as large as in the dipped method. However, after several passes of the rod on the string along the same wear track the friction forces became indistinguishable from those of a system produced by the dipping method.

The apparatus is sketched in Figure 2. The rod is pressed against the string, which is mounted on a frame on micrometer mounts that allow the normal force of the string on the rod to be adjusted. The rod is 250 mm long and 6 mm in diameter, mounted on an aluminum plate into which a semicircular groove has been machined. Electric heaters on the aluminum plate allow the rod to be heated. The rod and plate are moved by a constant velocity stage (Aerotech model ATS70030-U, Pittsburgh, PA, USA). In each run the carriage of the stage moves 0.2 m at a constant speed 0.2 m/s, with a peak-to-peak variation of about 5%. Acceleration and deceleration both occupy about 0.1 s, so all runs last slightly longer than 1 s. A violin E string is used: it is a high-tensile steel monofilament with a diameter of 270 μm and is stretched between two end supports 315 mm apart. The tension in the string is adjusted so it oscillates at 650 Hz, giving many hundreds of periods of oscillation in each run. The results obtained are found to be independent of whether the string is cleaned before each run.

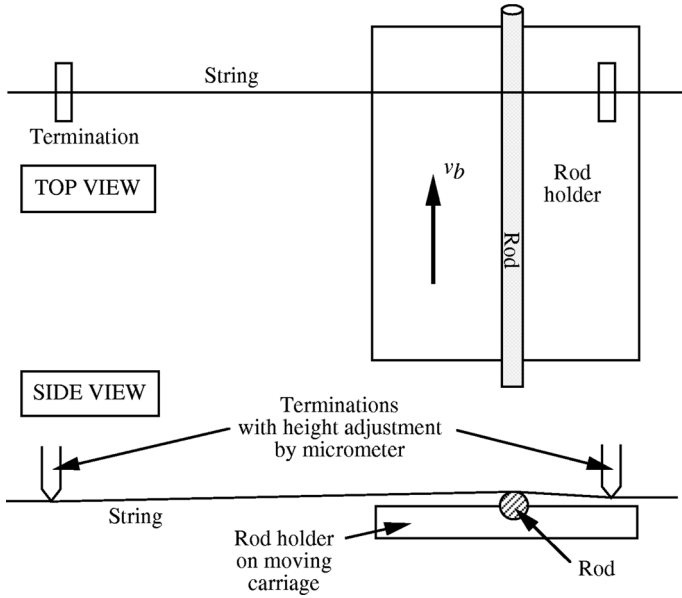

FIGURE 2 Sketch of the bowed-string apparatus (not to scale). Side view shows rod pressing on string to produce normal force.

Piezoelectric force sensors mounted at the string terminations measure the transverse component of the oscillating force exerted by the string, without interfering with the motion of the string. The conditioning amplifiers for these sensors have a low-frequency cutoff around 4 Hz to avoid drift problems. The terminating structures are designed to minimize energy losses to the mounting structure. The force signals are digitized at 128 kHz with 16-bit accuracy, to give adequate resolution of all relevant details.

Reconstruction

The friction force and string velocity in the region of contact are computed by a reconstruction method that uses the measured termination forces [16]. First, a range of calibration information is obtained by analyzing the force signals in response to free string vibration following a controlled pluck at the bowing point (with the bow not in contact with the string at this stage). These pluck results give the time delays of wave propagation to the two ends of the string, and also the bending stiffness of the string, the gains of the amplifiers, and the Q losses in the system (energy losses by the string and the mounting during

vibration). The decay of each individual normal mode after the pluck characterizes Q losses: $2\pi/Q_n$ is the fraction of energy in the nth mode lost per cycle of its vibration. All string modes have $Q_n > 1000$, some as high as 3000.

The reconstruction algorithm then combines the forces measured at the two terminations, using the parameters from the pluck experiments, to calculate the velocity, $v(t)$, of the center of the string, and the friction force, $F(t)$, at the bowing point. Each of these quantities can be calculated in two different ways, which provides a built-in check on the accuracy of reconstruction.

Because the string makes contact with the rod at its periphery, the time-varying friction force will also excite torsional motion of the string. This means that the velocity of the string's surface will be somewhat different from the reconstructed center velocity. An example showing very strong torsional motion was presented and analyzed in reference 16. This case arose from a resonant interaction with a torsional string mode. For the results to be shown here, resonant torsional motion has been avoided; nevertheless, some torsion is inevitably present and this slightly complicates the interpretation of results, as is discussed later.

Measurement of the Average Frictional Force and Normal Force

Because of the low-frequency roll-off of the measured force signals, the reconstruction of the dynamic friction force, $F(t)$, from the measured termination forces can only give the AC component. To obtain the DC component of the frictional force, an optical method has been developed. The DC frictional force, and also the normal force set by the micrometers, can be deduced from the displacement of the string at the point of contact with the rod. A force F, either in the plane of the string and the rod or in the direction normal to it, produces a deflection, d, conveniently expressed by

$$F = \frac{2Zd}{T\beta(1-\beta)} + \text{bending stiffness correction} \qquad (1)$$

where T is the period of oscillation, β is the fractional distance of the contact point to the nearer termination, and Z is the wave impedance of the string given by $Z = 2M/T$, where M is the total mass of the string between the terminations. For the string used here $Z = 0.17\,\text{kg/s}$. The bending stiffness correction turns out to be negligible for this very thin string (although it plays an important role in the reconstruction of AC force [16]). The normal force, N, is determined

directly from Equation (1) from the displacement given by the micrometers. For a 1 *N* force, the displacement of the string in these experiments is about 400 μm.

The lateral displacement caused by the average friction force during oscillation is measured with a video microscope oriented normal to the plane of oscillation of the string. The images are recorded during each run: about 22 periods of oscillation occur per video frame. The average position of the blurred image of the string at the bowing point is then determined from each individual frame of the recording, displayed against a calibrated reticle. The mean displacement of the string as a result of the frictional force typically lies in the range 40–150 μm in these experiments. The measured displacement from each frame then produces the DC component of the frictional force, F_{dc}, from Equation (1).

Advantages of the Bowed-String Method

The particular strengths of this new approach to friction characterization become apparent when the dynamics of bowed-string motion are examined. There are three major features to note.

(1) In the earlier experiments, the apparatus was supposed to vibrate with only a single degree of freedom. However, all physical systems have higher modes of vibration, and, because stick–slip motion generates forces with a wide frequency bandwidth, these higher modes make interpretation of results much more complicated. The stretched-string apparatus gets around this problem entirely: the string has many vibration modes, but they are all taken into account in the reconstruction algorithm. This allows useful data to be collected over the full audio-frequency bandwidth.

(2) A stretched string excited by bowing exhibits a very rich range of dynamical behavior, both periodic and nonperiodic. Different periodic regimes, transitions between these regimes, and nonperiodic transient behavior all yield data, which can shed light on many different aspects of the underlying frictional constitutive law. We present results relating to three types of periodic motion, and also from an unusual transient event. Each of these types of oscillation results in a characteristically different time-varying velocity and force on the friction point. Furthermore, the issue of which oscillation regime the string chooses under given conditions is a particularly challenging one for theoretical models, and, thus, these date provide a sensitive test. A friction model that could predict the correct sequence of oscillation regimes during this

kind of transient stick–slip test would have good claims to be convincing. At least for rosin, this is not an unrealistic objective: it has been shown that a skilled violinist can control the length and nature of initial transients with impressive consistency [17], so the inherent variability of frictional interfaces cannot be used as an excuse for poor models!

(3) The oscillation regime normally used by violinists is called the Helmholtz motion [18], and its form is quite counterintuitive. At any given instant, the string forms a V shape with two virtually straight segments joined by a sharp corner. This corner travels back and forth along the string, one round trip per period, tracing out the visible envelope of the string motion. As it passes the bow it triggers transitions between sticking and slipping friction, so that the motion has one sticking period and one slipping period per cycle. The timing is determined by the bowing position: in ideal Helmholtz motion there is sticking for a time $(1-\beta)T$ and slipping for the much shorter time βT every period. For our experiment, these times are approximately 1.35 ms and 0.15 ms, respectively. During sticking, the string moves at the speed, v_b, of the bow (0.2 m/s), whereas during slipping it moves at velocity $-v_b(1-\beta)/\beta$, about -1.8 m/s. Stick–slip motion based on a single-degree-of-freedom system behaves very differently: unless the normal force is very high, the interval of sticking is very short and the maximum slipping speed is approximately equal to the bowing speed (see, for example, reference 19). The result is that the bowed-string apparatus operates under a significantly different combination of force, speed, and timescale parameters and, therefore, yields data that can test theories in a different regime.

RESULTS AND DISCUSSION

Regimes of Oscillation

A typical example of the bowing-point velocity waveform for our experimental string during Helmholtz motion is shown in Figure 3a. The velocity axis is labeled in the coordinate system of the rod, so that the sticking velocity is zero. However, the measured velocity is not exactly zero for the sticking period: there are small-amplitude ripples that are discussed later. In Figure 3b we show the corresponding waveform of friction force $F(t)$. A striking feature of this plot is a negative one: the force waveform does not show any obvious distinction between sticking and slipping, although this is the dominant feature of the velocity waveform.

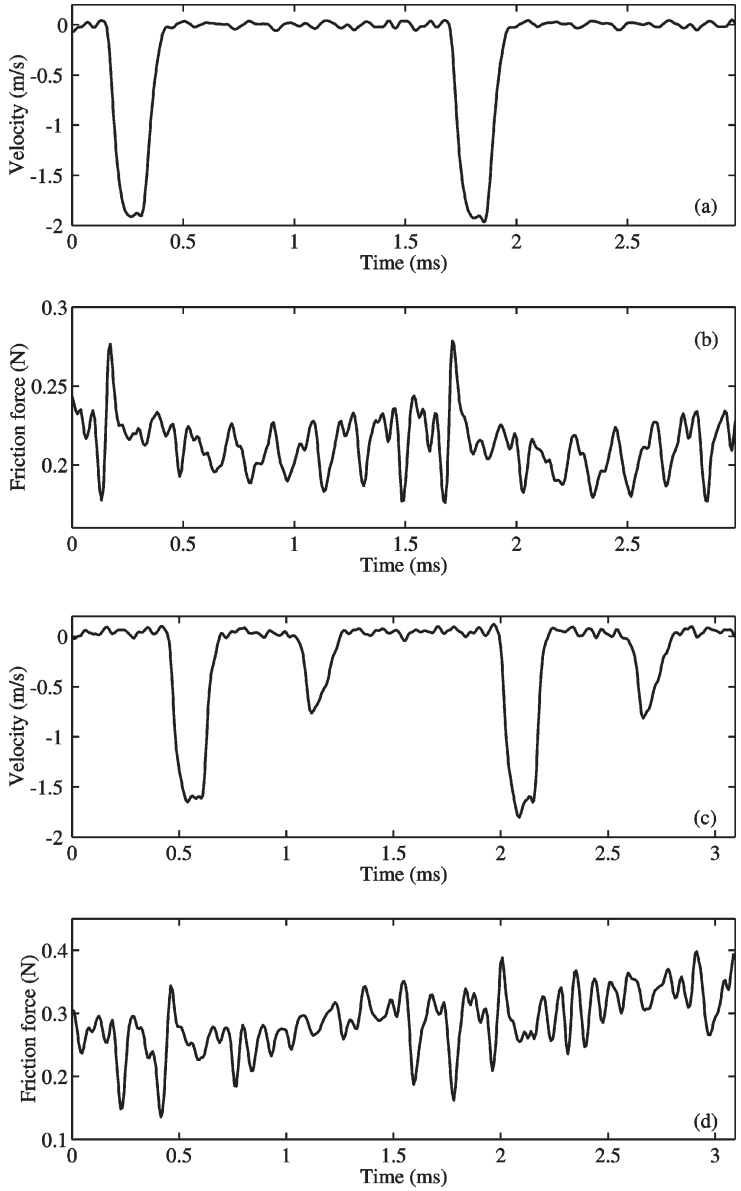

FIGURE 3 Waveforms of reconstructed velocity and force for three examples of string motion; (a, b) Helmholtz motion, with normal force 2.5 N and mean friction force 0.2 N; (c, d) double-slipping motion, with normal force 2.2 N and mean friction force 0.29 N; and (e, f) S motion, with normal force 4.1 N and mean friction force 0.4 N. Note the differing force and velocity scales. Measurements done at room temperature (22°C).

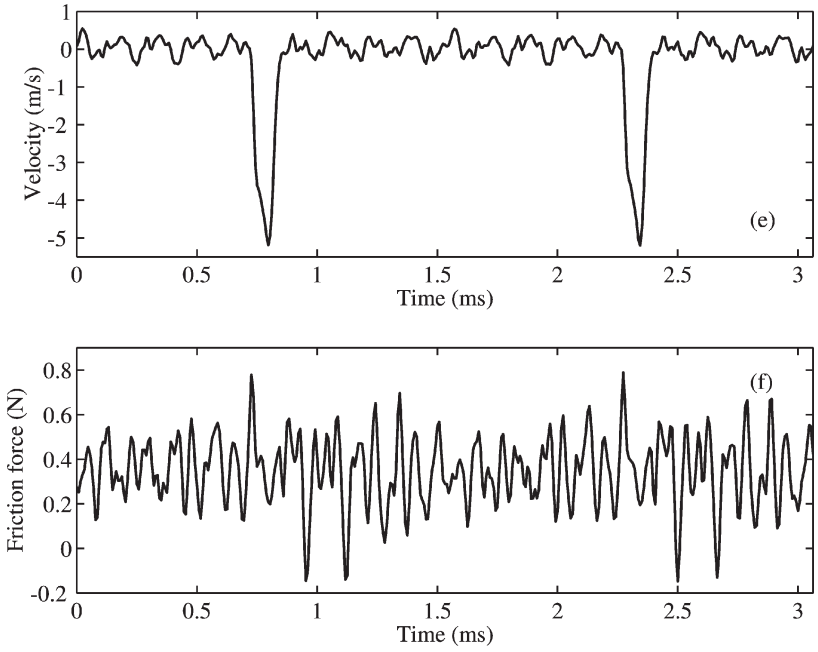

FIGURE 3 Continued.

In addition to Helmholtz motion, results are shown for two other types of string motion from the classification first developed in a famous article by C. V. Raman [20] in 1918: a double-slip oscillation and a particular Raman "higher type" denoted S motion [21]. Double-slip motion has two episodes of slipping per period, each of approximately the same duration as Helmholtz slips. It, therefore, has smaller slip velocity than in Helmholtz motion, because in any periodic motion the velocity of the string (in the reference frame of the fixture holding the string) must integrate to zero over a period. Animations of double-slipping motion and Helmholtz motion can be found in reference 22. Double-slipping motion is most often found either when the normal force is low [23] or during an initial transient. The smaller of the two slips then dies out as the string approaches its stable oscillating state, usually Helmholtz motion. The velocity and force waveforms for a typical example during such transient double-slipping motion are shown in Figures 3c,d: it is apparent that this example is not exactly periodic. However, the measurement method makes no assumption of periodic motion, so that it can produce useful results from all parts of a run.

S motion can most simply be described as a superposition of Helmholtz motion and a large-amplitude standing wave at mode number $n \approx 1/\beta$ [21]. The amplitude of this extra standing wave depends on the bowing position and often exceeds the amplitude of the first harmonic of the Helmholtz motion. In the current context, the most interesting consequence of S motion is that it has a single slip per period of very short duration, so that the maximum slipping speed is much higher than that of Helmholtz motion. Figures 3e,f show a typical example of the velocity and force waveform in S motion, with peak sliding speed more than double what was seen in Figure 3a.

An alternative presentation of the results of Figure 3 is to combine the two waveforms to plot the trajectory in the F-v plane, similar to Figure 1. A typical result, for the example of Helmholtz motion from Figure 3a, is shown in Figure 4. Toward the right-hand side is a near-vertical feature that corresponds to sticking, whereas during the interval of slipping there is a hysteresis loop similar to those found in earlier dynamic measurements [6, 11, 12]. The direction of travel around the loop is counterclockwise: there is high force at the start

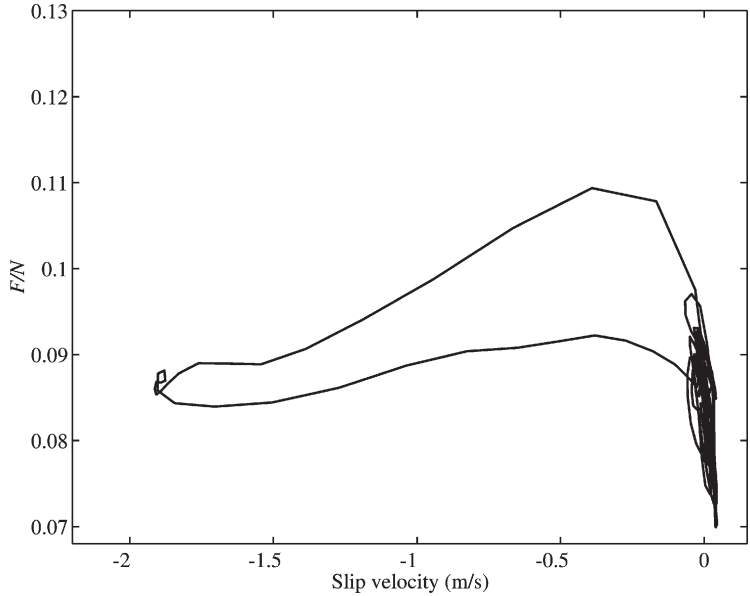

FIGURE 4 Trajectory in the F-v plane for the example of Helmholtz motion shown in Figure 3a,b. Friction force has been divided by normal force for ease of comparison with Figure 1.

of each slipping episode, reducing as the sliding speed increases, but not increasing to the same high level when sliding slows down and sticking resumes.

Figure 4 has been plotted with the friction force scaled by the normal force, so that the results can be compared quantitatively with Figure 1. It is immediately apparent that the values are much smaller in Figure 4, even though the friction material is essentially the same. The difference comes from the contact conditions. The axis in Figure 4 is deliberately not labeled "coefficient of friction" because this experiment is not operating in the familiar Coulomb friction regime in which the ratio F/N is constant. As is demonstrated in a later section, the contact conditions are such that one would expect it to be operating in the Hertzian contact regime for which in the ideal case friction force, F, would be proportional to $N^{2/3}$, so the ratio F/N would be proportional to $N^{-1/3}$ (see, for example, Johnson [24]). In other words, the contact has the nature of a large single asperity, not of a rough surface with multiple contacting asperities. With a smaller normal load, the value of F/N would be expected to rise from the low value seen in Figure 4, and this is the most likely explanation of the discrepancy with Figure 1: the experiment that generated Figure 1 used different contact geometry, leading to reduced contact pressure and, thus, to higher friction force.

As an aside, this observation about contact regime and typical friction force may explain why a violin string is normally bowed using a rosin-coated ribbon consisting of many separate strands of horsehair, rather than with a rod as in these tests. A friction force as low as one tenth of the normal force would make life difficult for a violinist. The ribbon of hairs in a conventional bow produces multiple contacts that will behave much like multiple asperities. This increases the real area of contact and, thus, gives a larger friction force that is more nearly linear with normal force over the range relevant in practice.

Sticking, Creep, and the Effect of Temperature

A universal feature of all F-v plots from this apparatus is that the velocity of the string at the bowing point never lingers exactly at zero during 'sticking,' as one might expect. Instead, a patch of "scribble" is seen, as in the lower right section of Figure 4. In the region where the friction force is highest, a curve is seen rather than a clear-cut transition that would allow one to define exactly when sticking stops and slipping begins. (The curve appears angular in the plot because the transition through this range is so fast that individual digital samples are seen, even with a sampling rate of 128 kHz. Such rapid

transitions are another unusual feature of this friction-measuring apparatus.) The maximum frictional force occurs when there is very significant relative motion between rod and string, at a rate of some 0.4 m/s for the case shown. The F-v plot is a useful way to examine the question "what, if anything, is sticking?" As is explained shortly, the detailed shape of the trajectory gives important clues about the associated physical processes.

There are two different types of process in operation when scribble is generated. First, as has already been pointed out, the friction force will generate some torsional motion of the string, which could give rise to rolling without violating the condition of sticking. The velocity reconstructed by this measurement method is of the center of the string (and also, therefore, of the center point of the contact region between string and rod). Rolling would show up in the waveform of center velocity, but in the context of F-v plots it would generate 'scribble,' which was simply an artifact, because F was being plotted against the "wrong" v. Because there can be no long-term cumulative rolling motion, this effect tends to produce scribble which is on average centered on the true sticking speed (zero in this reference frame).

However, although rolling undoubtedly accounts for some of the observed "sticking scribble," it is not the whole story. These experiments also show systematic deviations of the center of the scribble away from zero velocity, strongly suggesting that there is some genuine relative movement between the surface of the string and the glass core of the rod during the intervals of nominal sticking. In other words, the state commonly described as sticking is rather more elusive than the word suggests, with some deformation taking place in the rosin layer.

A series of measurements has been carried out in which the ambient temperature around the rod and friction-contact zone was systematically changed, and this gives the clearest evidence for deformation in the rosin layer during "sticking." The results shown in Figures 3 and 4 were obtained with ambient temperature around 22°C. When temperature was raised sufficiently, to around 60°C, self-excited vibration of the string was found to cease entirely, giving the first direct proof that temperature plays a role in the mechanics of 'stick–slip' friction mediated by rosin, as had been proposed previously on the basis of less-direct evidence [6, 7]. The most interesting behavior was seen at a temperature just a little lower, around 56°C. At this temperature the string remained almost stationary for the first half of the run, but then oscillation grew from small amplitude until, after some tens of period lengths, it settled into fairly normal-looking

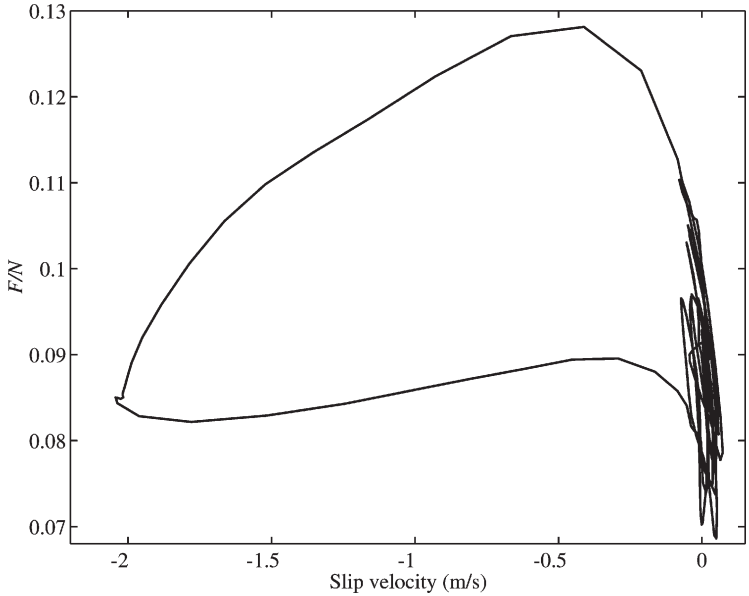

FIGURE 5 Trajectory in the F-v plane for Helmholtz motion at elevated rod temperature of 56°C. The normal force is 4.1 N, and the mean friction force is 0.4 N. Friction force has been divided by normal force for ease of comparison with Figures 1 and 4. Scales are the same as Figure 4.

Helmholtz motion. Figure 5 shows the F-v plot from the fully developed Helmholtz motion.

Figures 4 and 5 show significantly different shapes and sizes of loop during slipping, but more relevant for the present discussion is a difference of detailed shape in the sticking portions of the curves. Figure 5 shows some scribble, but it also shows a very clear systematic effect in which the curve through the middle of the scribble bends conspicuously toward the left at high friction force. Indeed, detailed inspection of the data of Figure 5 reveals a clear correlation between F and v throughout the sticking portion, each loop within the scribble having a definite tilt. A similar trend is found, rather less obviously, within the band of scribble in Figure 4.

The data from the "hot" run is even more striking when the transient part of the motion is examined. Figure 6a shows the velocity waveform during the growth phase of the oscillation. The waveform looks very much like the Helmholtz slip–stick pattern across the whole of this plot, but the 'sticking' speed (the plateau level near the top of the plot) is not constant, and on the left of the plot it is well below zero

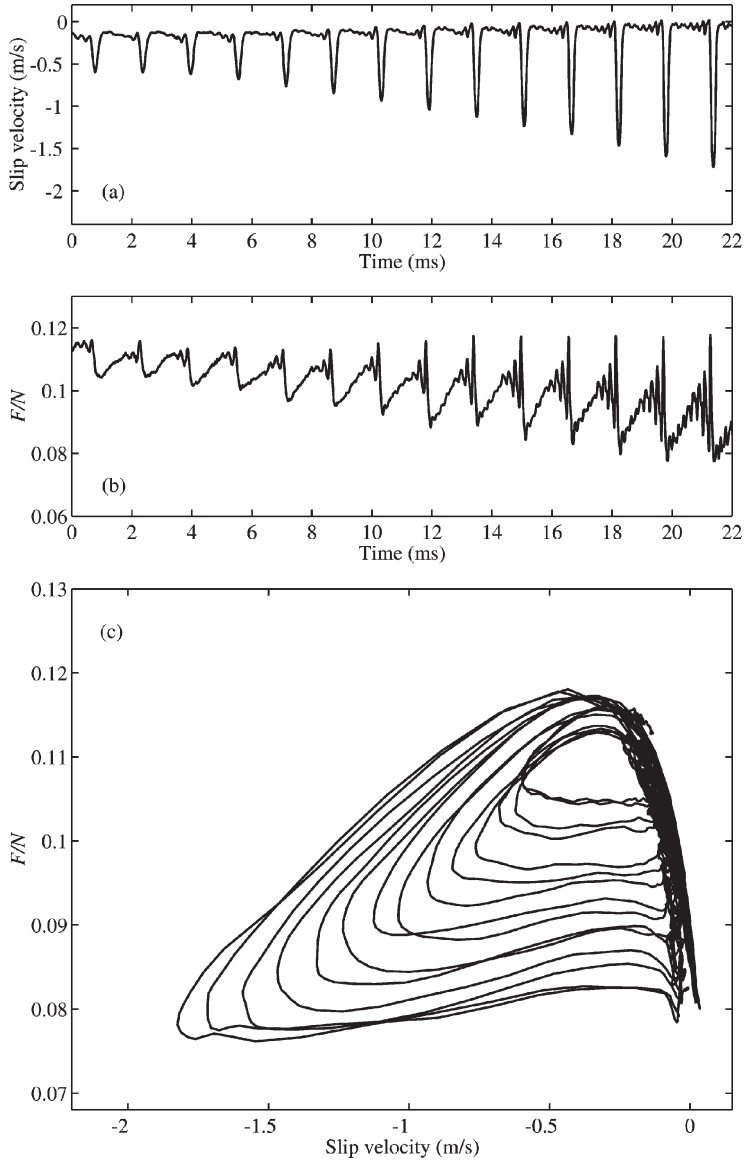

FIGURE 6 (a) Velocity waveform, (b) friction force, and (c) trajectory in the F-v plane for a transient period of the data shown in Figure 5, showing the growth of Helmholtz-like motion. For (c), friction force has been divided by normal force for ease of comparison with other figures. Each cycle of the oscillation traces a counterclockwise loop: loop size starts small and grows progressively during the transient motion. Scales are the same as Figure 4.

(the speed of the rod). How can there be sticking under those conditions? This counterintuitive pattern becomes more understandable when the friction-force plot is examined, as shown in Figure 6b. During the growth of the oscillation the mean value of friction force falls by a significant factor: before the oscillation started, the mean friction force was about 0.5 N, and by the time the Helmholtz motion is fully established, this has fallen by 20% to 0.4 N.

When the velocity and force data are put together into the F-v plot, as in Figure 6c, an outward-spiraling series of loops is traced out by successive cycles, but these all have their sticking portions lying on essentially the same curve. The small loops, associated with the earlier part of the transient growth, have sticking speeds that are significantly negative, as was seen in Figure 6a. However, this variation in 'sticking' speed can now be seen to be correlated with the decrease in DC frictional force, following essentially the same tilting curve identified in Figure 5 from the fully developed Helmholtz motion.

It must be admitted that this observation of a common backbone curve during 'sticking' is somewhat speculative, because of uncertainties arising from the inherent errors associated with the video analysis for measuring the DC force. A skeptical reader may question whether the evidence of Figures 5 and 6 is clear enough to be compelling. The problem is that the transient examined here occupies a total time that is less than one frame of the video analysis, so that the method can only yield a rather coarse and approximate version of the DC force during a transient like this, based on interpolation between relatively sparse neighboring data points. More and better data need to be gathered to test the interpretation suggested here, but, nevertheless, these results give an intriguing clue about a possible physical model of the processes taking place within the rosin layer, which is worth comment.

A possible interpretation of these results is to suggest that the 'sticking' periods involve some kind of viscous flow in the rosin layer, with a shear force strongly correlated with velocity or shear strain rate. It would be natural to call this viscous flow "creep," except that it should be noted that with the speed and layer thickness relevant here, the strain rate is of the order of $10^5\,\mathrm{s}^{-1}$. This enormous strain rate is by no means what would usually be called creep, and indeed it rivals the highest strain rates that can be obtained in measurement rigs involving projectiles and shock-wave generation!

The slope of the curve in Figure 6c can be used (together with information about the contact size) to deduce an effective creep viscosity. The shape of the curve then clearly indicates a nonlinear relation

between viscosity and shear rate (a relation that also varies with ambient temperature). Crucially, there appears to be some kind of softening behavior in which the shear viscosity (*i.e.*, the slope of the curve) is lower when the shear rate is higher. But softening behavior of this general kind is well known to lead to instability involving the formation of a localized shear band, as has been observed in a range of different materials and systems (see, for example, references 25 and 26). Could an instability of this kind give a basis for a transition between two states, which we might label "sticking with creep" and "gross sliding?"

The speculative model might run as follows. When the shear stress or strain reaches a critical level, softening behavior (linked to temperature rise [26]) would lead to the formation of an unstable localized shear band somewhere within the thickness of the rosin layer. When the instability takes hold, there would be a short period during which the pattern of deformation adjusts to become concentrated in the shear band: this would correlate with the rounded peak seen in all the F-v plots surrounding the maximum friction force, where, as already commented, the change is so rapid that individual digital samples are seen in the plots.

There would then follow an episode of gross sliding during which the deformation was largely confined to a very thin interfacial layer, with consequent large temperature changes [6, 7]. During such gross sliding there is no clear evidence that sliding velocity is a major controlling variable, and a model involving a temperature-dependent interfacial shear strength as presented by Smith and Woodhouse [6] may be appropriate. Gross sliding would come to an end when the kinematics of the string motion led to the total shear-strain rate dropping back to a value near zero, so that the shear band might "heal" and "sticking with creep" resume.

This picture seems to be consistent with all the major features of the results presented here, and also to have the potential to resolve an unsatisfactory conflict between two models for rosin friction proposed earlier [6]: a 'viscous model' and a 'plastic yield model,' both of which were shown to have promising features. Under this new picture, both those models could be relevant, applying in different parts of the motion as a shear band forms and heals within the rosin layer at a frequency of hundreds of Hertz. To explore these ideas further requires new modeling and simulation and is a goal for future work. The model could possibly be relevant not only to rosin but also to other viscoelastic materials or non-Newtonian fluids for which experiments have suggested some kind of "yield fluid" constitutive law (see, for example, reference 27).

Wear Tracks and Contact Size

Further evidence that bears upon the question of what happens during sticking can come from an examination of the wear tracks left in the rosin coating on the rod after a single pass over the vibrating string. A typical SEM micrograph is shown in Figure 7a. This micrograph is reproduced from reference 16 (Figure 8a). It is not from the same run as any of the earlier figures shown here, but it is chosen because it illustrates a variety of interesting features in a single picture. For this particular oscillation regime, there were two slips per period with a very brief sticking interval between. That accounts for the alternating pattern of the sticking scars. The regions marked A and B are the undisturbed surface of the rosin coating. The scars below letters A were created during the longer of the two sticking periods in each cycle of the string motion, and those below B during the shorter sticking periods. The wider spreads (horizontal in the figure) of the scars under A compared to those under B reflects this difference of sticking time: longer sticking means that more contact movement, whether rolling or creeping, can occur. Debris has been projected some distance from the track. The regions marked C are slipping tracks. D marks an area of adhesive failure, where the rosin has either been removed entirely from the glass surface, or has left only a very thin layer behind.

In Figure 7b (an enlargement of part of Figure 7a), the region of adhesive failure is more clear. E marks debris created possibly by cohesive failure, F marks fracture cracks on a piece of debris, and G shows a region with a texture highly suggestive of the phenomenon known as the "printer's" or "ribbing" instability: see, for example, reference 28. Thus, the rosin shows both brittle fracture characteristic of a glass and viscous flow characteristic of a fluid. This mixture of behaviors in such close proximity is strongly suggestive of temperature-induced material changes.

To relate these wear tracks to the information obtained from the friction-force reconstruction it is useful to plot the force results in a different way. By integrating the velocity signal, friction force can be plotted as a function of distance, x, along the rod surface. Note that in this case there is no uncertainty resulting from torsional motion of the string; the reconstructed velocity corresponds precisely to the motion of the center of the contact patch between rod and string. Figure 8a shows $F(x)$ for two typical cycles during the Helmholtz motion of Figure 3a.

Figure 8b shows an enlarged view of the center sticking region of Figure 8a. Unfortunately, there is some uncertainty in this region

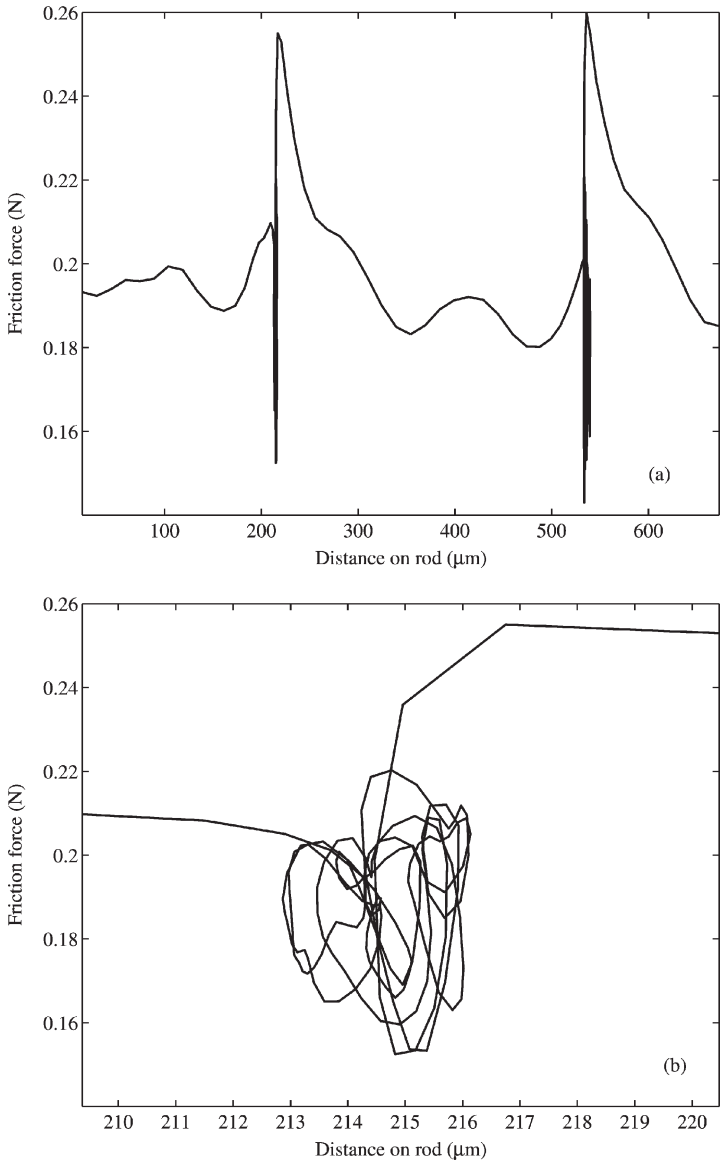

FIGURE 8 (a) Friction force as a function of position along the surface of the rod, for the Helmholtz motion of Figure 3a, and (b) magnification of one sticking episode of (a).

because the instantaneous rod velocity is perturbed by small-amplitude oscillations of the moving carriage drive system. To plot this version of the figure, a value has been chosen for the rod velocity, within the known error bounds, which minimizes the lateral extent of the motion during sticking. This may mean that cumulative drift resulting from creep has been removed. Despite this uncertainty, some features visible here are clearly characteristic of the sticking of the string to the rod. Complex motion of the center of the string during sticking is evident, although whether this arises from rolling, creep, or a mixture of both cannot be resolved from this evidence alone.

The extent of movement of the sticking region revealed by Figure 8b is only some 3 μm, much less than the physical size of the sticking scars seen in the micrographs. Part of the reason may be missing cumulative creep, as just mentioned, but it must also be remembered that the physical scar corresponds, more or less, to the entire region over which there was some contact between the rod and the surface of the string during the sticking interval. The size of this region is influenced not only by movement of the center of the contact, but also by effects of local deformation caused by the contact forces. Even if effects resulting from the relatively soft rosin layer are ignored, we have contact between two crossed cylinders of glass and steel. The form of local deformation under such conditions is well known, from the classical work of Hertz (see, for example, Johnson [24], Chapter 4). The contact zone is an ellipse with dimensions determined by the radii of the two cylinders and their respective Young's moduli of elasticity. Carrying the calculation through with appropriate parameter values for the string and the glass rod yields a contact region that for a normal force of 4 N has approximate dimensions $160 \times 20\,\mu\text{m}$, which is of the same order as the typical dimensions of the narrowest observed sticking scars.

From the same Hertz contact calculation, it is also straightforward to calculate the contact-pressure distribution: the average pressure for a normal force of 4 N is 1.5 GPa, with a distribution over the contact zone that rises from zero around the edge to a peak value above 2 GPa at the center. These pressures are enormous compared with any reasonable estimate for the compressive yield stress of a substance like rosin, and this serves to justify a comment made earlier. With pressures this high, any asperities resulting from surface roughness of the glass rod, rosin coating, or the steel string are irrelevant because the rosin layer yields locally, leading to fully conforming contact over most the Hertzian ellipse.

Energy Dissipation

A final topic of interest is the energy balance involved in frictionally excited oscillation. The energy flowing from the string to the rod (considered positive here) is

$$E(t) = -\int_0^t [v(\tau) - v_b][F(\tau) + F_{\mathrm{dc}}]d\tau \tag{2}$$

where the minus sign appears because the forces in the integrand are forces on the string by the rod. This integral can be evaluated directly from the data. For the frictional forces in this run, the energy flow E is about 92 μJ/period (60 mW) for $F_{\mathrm{dc}} = 0.3$ N. Figure 9 shows $E(t)$ for the Helmholtz motion shown in Figures 3 and 4. The plot takes the form of a "staircase": the steep portions indicate the intervals of slipping, whereas the almost-horizontal portions indicate intervals of sticking. It is immediately apparent that the energy input is much larger during the slipping portion of the cycle than during the sticking portion. The small slopes seen during the sticking portion are mainly within the experimental uncertainties caused by variations of the instantaneous bow velocity.

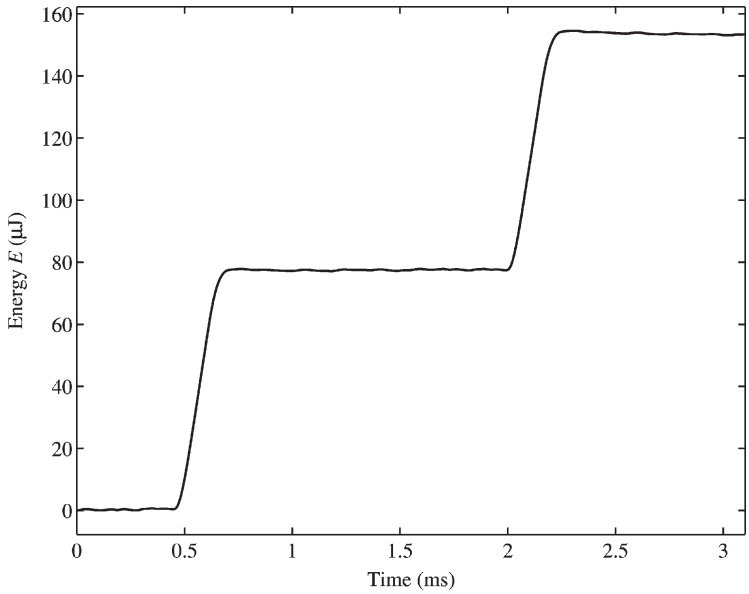

FIGURE 9 Energy to the rod from the string as a function of time, for Helmholtz motion of Figure 3a.

During steady periodic motion of the string there is no change in the sum of kinetic and potential energies, and the energy flowing across the frictional interface is all dissipated somewhere in the system. This energy dissipation can be separated into four channels:

$$E = E_{\text{string}} + E_{\text{rig}} + \gamma\,\Delta A + E_{\text{layer}}. \tag{3}$$

E_{string} is the energy loss into the string vibration, associated with the dissipation at the string's terminations, by air resistance, and so on: in other words, it is the energy required to maintain the string oscillation when the rod is not in contact with the string. E_{rig} is the corresponding energy loss into the rig on the other side of the contact region: the rod, trolley, and so on. The term $\gamma\,\Delta A$ is the energy needed to create the new surface area, where γ is the surface energy of the rosin layer and ΔA is the newly created area of the rosin/air interface. We define E_{layer} to be the energy required to reshape and move the rosin material, as shown in the wear track of Figure 7.

It is straightforward to estimate the energy dissipated into the first three loss channels. E_{string} is deduced from the measured Q factors of the normal modes from the pluck results. By using the Fourier decomposition of ideal Helmholtz motion (Helmholtz [18], Appendix VI) these Qs can be combined to give a total energy-loss rate from free vibration. We have included in this calculation all string modes up to 20 kHz, which will give a slight overestimate of the actual energy loss because higher modes will be excited less strongly in practice than in the ideal case. The result is $E_{\text{string}} \approx 2.3\,\text{nJ/period}$ ($\approx 1.5\,\mu\text{W}$), several orders of magnitude smaller than the total energy transfer measured previously. (This disparity of magnitudes was noted, in less detailed form, by Cremer [29], Section 3.6.) The corresponding term E_{rig} is less easy to determine quantitatively, but the vibration modes of the rig have Q factors that are in general lower than those of the string; the mass of the rig is much higher than the string, and its modal density is lower, so one can confidently predict that E_{rig} will be at most of the same order of magnitude as E_{string}.

We can also estimate the energy lost in creating new surface area. We assume γ is on the order of $0.06\,\text{J/m}^2$ (a number typical of a polar organic material such as rosin [13]) and $\Delta A \approx 0.036 \times 10^{-6}\,\text{m}^2/\text{period}$ as estimated from the wear track. We then find that this loss channel is about $2.2\,\text{nJ/period}$ ($\approx 1.5\,\mu\text{W}$). Thus, this channel is also a negligible fraction of the energy used in the system. We are left with the fact that E_{layer}, energy used to disrupt the rosin layer, accounts for almost all energy dissipation in the system. Furthermore, virtually all of that energy is dissipated during the slipping portion of the oscillation.

DISCUSSION AND CONCLUSIONS

We have described an experimental approach to the characterization of dynamic friction force using an apparatus based on a stretched string excited by a "bow" consisting of a glass rod coated with the desired friction material, rosin for the results shown here. Stick–slip oscillations of the string are excited by moving the rod with a known velocity, and the friction force and the string velocity at the point of contact with the rod are inferred by processing of the signals from non-intrusive force transducers at the two ends of the string. We argue that an inverse measurement of this general kind is the best way to gather reliable data on the behavior of interfacial friction in this high-frequency dynamic regime, which is important to many engineering applications.

The bowed string is a good system to use for this purpose, because it is well understood compared with other systems that exhibit frictionally excited vibration. It offers several advantages compared with the single-degree-of-freedom systems that have been used in the past. All the modes of the string are taken into account in the processing, so that there is no problem associated with unwanted higher modes of the apparatus. This greatly extends the useful frequency bandwidth of data. Another advantage of the bowed string is that it operates in a regime that falls in a different region of the parameter space relating to contact conditions (normal force, sliding speed, rate of change of sliding speed, etc.). This means that it can gather data complementary to other methods. Finally, the string exhibits very rich dynamical behavior, showing a range of different characteristics. The method used here makes no assumptions about the form of motion, so it can provide useful data from different regimes of periodic motion, from transitions between such regimes, and from nonperiodic motion during initial transients or extended spells of chaotic motion. These data throw down a gauntlet to the modelers to develop a frictional constitutive model that can reproduce quantitatively the rich range of behavior revealed.

The results of the friction-force measurement can be correlated with microscopic examination of the wear track left on the surface of the rod after a single pass over the string. This gives additional insight into the physical processes governing the friction force. These processes have been shown to be complicated. The wear tracks exhibit a wide range of different features: brittle fracture, ductile failure, viscous flow, and the generation of and interaction with wear debris.

The results shown here, and others published previously using the same friction material [6, 7, 9], demonstrate that dynamic friction in

this system is not fully captured by any of the friction models so far proposed. It has been directly confirmed that temperature plays a significant role for this friction material. At sufficiently high ambient temperature, stick–slip motion ceases entirely. Data have been shown at a temperature when self-excited vibration becomes marginally possible, and the results compared with those at lower temperature when stick–slip motion is ubiquitous.

Strong evidence has been shown for temperature-dependent shear flow in the rosin layer during sticking. It has been suggested that a nonlinear viscous model might be a promising candidate to account for the observations, and that the transition to slipping might arise from an instability, perhaps associated with material softening, leading to the formation of a shear band [25, 26]. During slipping, it has been shown that a different type of governing law is needed for the friction force, because sliding velocity is not strongly correlated with force. Temperature within a thin interfacial layer is a strong candidate.

These results and conclusions suggest a range of further research that may be fruitful to advance understanding of the initiation and waveforms of frictionally excited vibration. A variety of further experiments could be valuable, using the test rig described here. More and better data are needed on the effects of ambient temperature to test the speculations advanced here. The friction material, normal force, sliding speed, and vibration frequency could all be varied with advantage. More careful analysis is needed of the regime of oscillation chosen by the string under different conditions. All this information then needs to be compared with simulation studies similar to those already reported by Woodhouse [7]. Simulation offers the most direct route to explore alternative constitutive laws for friction, such as the one proposed here. Rational design strategies to control stick–slip vibration in practical situations might then become possible.

ACKNOWLEDGMENTS

The authors thank K. L. Johnson, J. A. Williams and C. Y. Barlow for helpful discussions on this research.

REFERENCES

[1] Akay, A., The acoustics of friction, *J. Acoust. Soc. Amer.* **111**, 1525–1548 (2002).

[2] Johnson, K. L., Dynamic friction, in *Tribology Research: From Model Experiment to Industrial Problem*, G. Dalmaz, A. A. Lubrecht, D. Dowson, and M. Priest (Eds.) (Elsevier Science, Amsterdam, 2001), pp. 37–45.

[3] Urbakh, M., Klafter, J., Gourdon, D., and Israelachvili, I., The nonlinear nature of friction, *Nature* **430**, 525–528 (2004).

[4] Ruina, A., Slip instability and state variable laws, J. Geophys. Research 88, 10359–10370 (1983).
[5] Heslot, F., Baumberger, T., Perrin, B., Caroli, B., and Caroli, C., Creep, stick–slip, and dry-friction dynamics: Experiments and a heuristic model, Phys. Review E 49, 4973–4988 (1994).
[6] Smith, J. H. and Woodhouse, J., The tribology of rosin, J. Mech. Phys. Solids 48, 1633–1681 (2000).
[7] Woodhouse, J., Bowed string simulation using a thermal friction model, Acustica—Acta Acustica 89, 355–368 (2003).
[8] Duffour, P., Noise generation in vehicle brakes, Doctoral thesis, University of Cambridge, UK (2002).
[9] Galluzzo, P. M., On the playability of stringed instruments, Doctoral thesis, University of Cambridge, UK (2003).
[10] Mills, K., ASM Handbook: Fractography V. 12 (ASM International, Metals Park, OH, 1991).
[11] Bell, R. and Burdekin, M., A study of the stick–slip motion of machine tool feed drives, Proc. Inst. Mech. Engrs. 184, 543–560 (1969–70).
[12] Brockley, C. A. and Ko, P. L., Quasi-harmonic friction-induced vibration, Trans. ASME J. Lub. Tech. 92, 550–556 (1970).
[13] The Merck Index, 9th edition, M. Windholz, S. Budavari, L. Stroumtsos, and M. Fertig (Eds.) (Merck & Co., Rahway, NJ, 1976), p. 1071.
[14] Schumacher, R. T. and Woodhouse, J., The transient behavior of models of bowed-string motion, Chaos 5, 509–523 (1995).
[15] Woodhouse, J. and Galluzzo, P. M., The bowed string as we know it today, Acustica—Acta Acustica 90, 579–589 (2004).
[16] Woodhouse, J., Schumacher, R. T., and Garoff, S., Reconstruction of bowing point friction force in a bowed string, J. Acoust. Soc. Amer. 108, 357–368 (2000).
[17] Guettler, K. and Askenfelt, A., Acceptance limits for the duration of pre-Helmholtz transients in bowed string attacks, J. Acoust. Soc. Amer. 101, 2903–2913 (1997).
[18] Helmholtz, H. von, Lehre von den Tonempfindungen (Braunschweig 1862); English edition: On the sensations of tone (Dover, New York, 1954).
[19] Den Hartog, J. P., Forced vibration with combined Coulomb and viscous friction, Applied Mech. 53, 107–115 (1933).
[20] Raman, C. V., On the mechanical theory of vibrations of bowed strings, Indian Assoc. Cult. Sci. Bull. 15, 1–158 (1918).
[21] Lawergren, B., On the motion of bowed violin strings, Acustica 44, 194–206 (1980).
[22] Woodhouse, J. and Galluzzo, P. M., Why is the violin so hard to play? Plus 31 October 2004, http: ==plus.maths.org =issue31=features =woodhouse=index.html (online magazine of the Millennium Mathematics Project).
[23] Schelleng, J. C., The bowed string and the player, J. Acoust. Soc. Amer. 53, 26–41 (1973).
[24] Johnson, K. L., Contact Mechanics (Cambridge University Press, Cambridge, UK 1985).
[25] Bai, Y. L. and Dodd, B., Adiabatic Shear Localization (Pergamon, Oxford, 1985).
[26] Swallowe, G. M. (Ed.), Mechanical Properties and Testing of Polymers (Kluwer Academic, Dordrecht, 1999), Chapters 3, 4.
[27] Bingham, E. C., Fluidity and Plasticity (McGraw-Hill, New York, 1922).
[28] Lopez, F. V., Pauchard, L., Rosen, M., and Rabaud, M., Non-Newtonian effects on ribbing instability threshold, J. Non-Newtonian Fluid Mech. 103, 123–139 (2002).
[29] Cremer, L., The Physics of the Violin (MIT Press, Cambridge, MA, 1985).